Supporting Information

Multi-Functional Dendrimer Ligands for High-Efficiency, Solution-Processed Quantum Dot Light-Emitting Diodes

Ikjun Cho, †, § Heeyoung Jung, ‡, § Byeong Guk Jeong,⊥ Jun Hyuk Chang, # Younghoon Kim, † Kookheon Char, # Doh C. Lee, ⊥ Changhee Lee, ‡ Jinhan Cho,† and Wan Ki Bae*,¶*

[§]These authors contributed equally to this work.

[†]Department of Chemical and Biological Engineering, Korea University, Seoul 02841, Republic of Korea

[‡]School of Electrical and Computer Engineering, Inter-University Semiconductor Research Center, Seoul National University, Seoul 08826, Republic of Korea

[⊥]Department of Chemical and Biomolecular Engineering, Korea Advanced Institute of Science and Technology (KAIST), Daejeon 34141, Republic of Korea

[#] School of Chemical and Biological Engineering, The National Creative Research Initiative Center for Intelligent Hybrids, Seoul National University, Seoul 08826, Republic of Korea

[¶]Photoelectronic Hybrids Research Center, Korea Institute of Science and Technology (KIST), Seoul 02792, Republic of Korea

1. Experimental methods

Chemicals: Zinc acetate ($Zn(acet)_2$, 99.99%, metals basis), 1-octadecene (ODE, 90%) and tri-n-octylphosphine (TOP, ≥ 99%) were purchased from UniAm (Korea). Cadmium oxide (CdO, 99.95%, metals basis), Se (99.99%, powder), S (99.998%, powder), oleic acid (OA, 90%), 1-dodecanethiol (DDT, ≥98%), and myristic acid (MA, ≥ 99%) were obtained from Alfa Aesar. Poly(amidoamine) dendrimers, ethanolamine (99.5 %), and 2-methoxyethanol (99.8 %) were acquired from Sigma-Aldrich. All organic solvents were used as received from Daejung (Korea) without purification.

QD Precursors: Cationic precursors (0.5 M cadmium oleate ($Cd(OA)_2$) and 0.5 M zinc oleate ($Zn(OA)_2$)) were prepared by degassing 100 mmol of CdO (or $Zn(acet)_2$) in a mixed solution of 100 mL of OA and 100 mL of ODE at 110 ^oC for 2 hr, followed by back-filling with Ar. The reaction flask was then heated up to 250 ^oC for 1 hr, degassed at 110 ^oC for 2 hr, and back-filled with Ar. Anionic precursors [2 M selenium in tri-n-octylphosphine (TOPSe) and 2 M sulfur in tri-n-octylphosphine (TOPS)] were prepared by dissolving 20 mmol of selenium and sulfur power in 10 mL of TOP under Ar atmosphere at 100 ^oC for 1 hr. 0.5 M DDT precursor was prepared by diluting 10 mmol of DDT in ODE with a total volume of 20 mL.

Synthesis of QDs: All QD synthesis was conducted with a typical Schlenk line technique under Ar atmosphere.[S1-S4] For CdSe (r = 2 nm)/CdS (h = 6 nm) QDs,[S1] we first synthesized a CdSe core with a radius of 2 nm and separately conducted CdS shelling by supplying desired amounts of 0.5 M $Cd(OA)_2$ and 0.5 M DDT into the reaction vessel containing the CdSe core solution (1 g of CdSe core in 15 mL of ODE) at a rate of 2 mL/hr. The reaction temperature was maintained at 300 ^oC throughout the CdS shelling process. CdSe (r = 2 nm)/$Cd_{1-X}Zn_XS$ (h = 6 nm) red QDs,[S2] $Cd_{1-X}Zn_XSe$ (r = 1.5 nm)/ZnS (h = 6.2 nm) green QDs,[S3] and $Cd_{1-X}Zn_XS$ (r = 2 nm)/ZnS (h = 2.3 nm) blue QDs[S4] were synthesized by one-pot synthetic methods. The resultant QDs were purified five times *via* the precipitation/redispersion method and dispersed in toluene for further experiments.

Device fabrication*:* ZnO films were prepared using a previously reported method[S5] with minor modifications. Prior to film formation, ZnO precursor was prepared by dissolving 1 g of $Zn(acet)_2$ and 0.28 g of ethanolamine in 10 mL of 2-methoxyethanol for 12 hr. The

resulting ZnO precursor was spun-cast on patterned ITO substrates with a spin rate of 3000 rpm for 30 s to form ZnO films. The ZnO films were then annealed at 300 °C under air for 1 hr. PAD ligand layers were formed on the ZnO film by spin-casting PAD ligand solutions diluted in ethanol (2 mg/mL) with a spin-rate of 4000 rpm for 30 s. The weakly bound PAD ligands were washed by spin-casting PAD//ZnO substrates with pure ethanol under the same spin condition. QD dispersions (20 mg/mL in toluene) were then deposited on PAD//ZnO substrates at 4000 rpm for 30 s, followed by a washing step (spin-casting with pure toluene). CBP, MoO_x, and Al electrode layers were thermally evaporated under a vapor pressure of 2×10^{-6} torr onto QD//PAD//ZnO//ITO substrates at deposition rates of 0.8–1 $Å \cdot s^{-1}$, 0.3 $Å \cdot s^{-1}$, and 4–5 $Å \cdot s^{-1}$, respectively. For solution-processed QLEDs, Poly(9-vinylcarbazole) (PVK) dissolved in chlorobenzene at a concentration of 15mg/mL was spun-cast onto QD//PAD//ZnO//ITO substrates at 3000 rpm for 60 s and annealed at 140 ° C for 30 min under Ar atmosphere, followed by thermal evaporation of MoO_x and Al electrodes.

Optical Characterization: UV-vis absorption and photoluminescence spectra were obtained with a Lambda 35 spectrometer (PerkinElmer) and Fluoromax-4 spectrometer (Horiba Science), respectively. The absolute PL QYs of film samples were obtained at an excitation wavelength of 450 nm with a C11347-01 (Hamamatsu Photonics). To characterize the PL decay dynamics, the samples were excited at 450 nm (pulse width = 80 ps) at a repetition rate of 1.0 MHz, and PL dynamics were resolved using a time-correlated single-photon counting (TCSPC) system that consists of a single channel analyzer (with a Picoquant Timeharp 260) and avalanche photodiodes (Picoquant τ-SPAD, timing resolution = 350 ps).

Film Characterization: The adsorption of QDs onto PAD-coated substrates and the traces of oleic acid ligands were qualitatively investigated using fourier transform infrared spectroscopy (FT-IR) in attenuated total reflection (ATR) mode (Agilent Technologies Cary 600 Series). Additionally, a quartz crystal microgravimetry (QCM) device (QCM200, SRS) was employed to quantitatively investigate the mass of PAD-G*n* (*n* = 0, 1, 3, 5) onto adsorbed ZnO films. The mass change (Δm) of the adsorbed PAD was calculated from the change in the QCM frequency (ΔF), using the Sauerbrey equation.[S8]

$$\Delta F(Hz) = -\frac{2F_0^2}{A\sqrt{\rho_q \mu_q}} \cdot \Delta m$$

where F_0 (5 MHz) is the fundamental resonance frequency of the crystal, A is the electrode area, and ρ_q (2.65 g·cm^{-3}) and μ_q (2.95 × 10^{11} g·cm^{-1}·s^{-2}) are the shear modulus and density of quartz, respectively. As reported in our previous paper,[S8] this equation can be simplified as follows

$$\Delta F\ (Hz) = -\ 56.6 \times \Delta m_A,$$

where Δm_A is the mass change per quartz crystal unit area in μg·cm^{-2}.

The surface morphologies of the films (*i.e.*, ZnO and/or PAD-G*n*//ZnO) were investigated with non-contact mode of atomic force microscopy (AFM) (XE-100, Park System). X-ray photoelectron spectroscopy (XPS) measurements were performed with a ULVAC-PHI X-tool Spectrometer (base pressure of 6.7 × 10^{-7} Pa) equipped with monochromatic Al-Kα X-ray photons ($h\nu$ = 1486.6 eV). Ultraviolet photoelectron spectroscopy (UPS) measurements were conducted with an AXIS-NOVA and Ultra DLD using a He I (21.2 eV for UPS) discharge lamp.

Device Characterization of QLEDs: The current–voltage–luminance (I–V–L) characteristics of the devices were measured with a Keithley-236 source-measure unit, a Keithley-2000 multimeter unit coupled with a calibrated Si photodiode (Hamamatsu S5227-1010BQ) and a photomultiplier tube detector. The luminance and efficiencies of QLEDs were calculated from the photocurrent measurement data obtained with the Si photodiode. The electroluminescence spectra were obtained using a spectroradiometer (CS-2000).

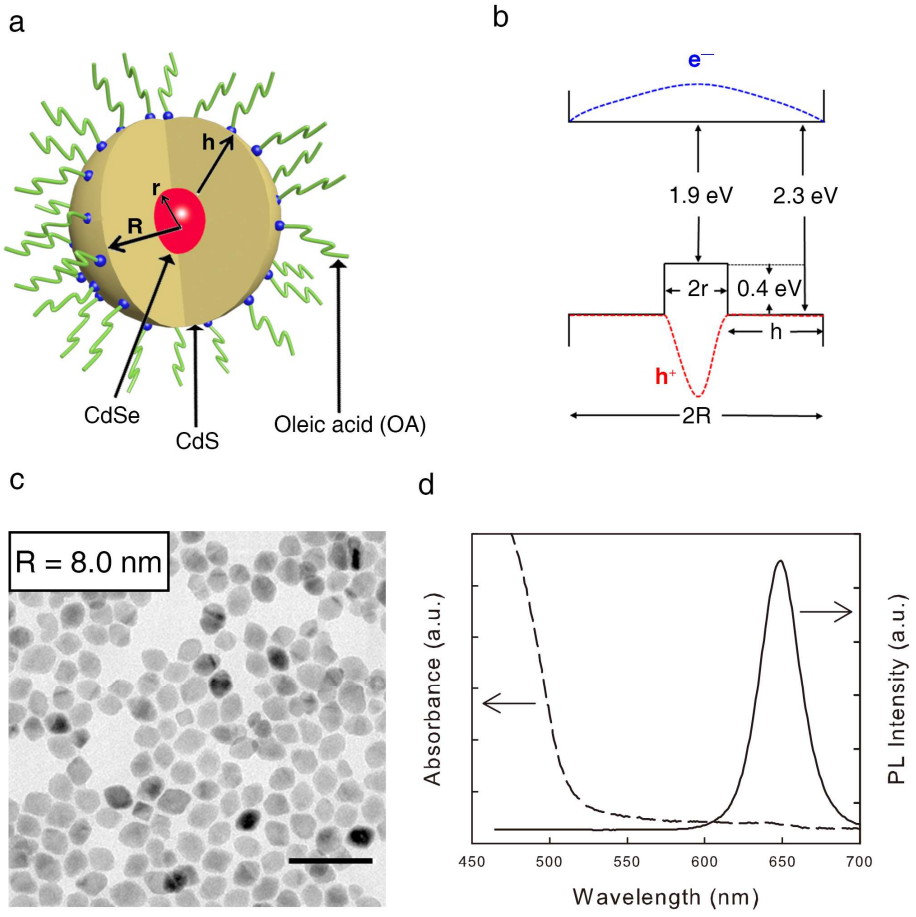

Figure S1. (a) Schematic illustration, (b) energy band diagram, (c) high-resolution TEM image, and (d) absorbance and PL spectra of of CdSe(r = 2 nm)/CdS (h = 6 nm) QDs.

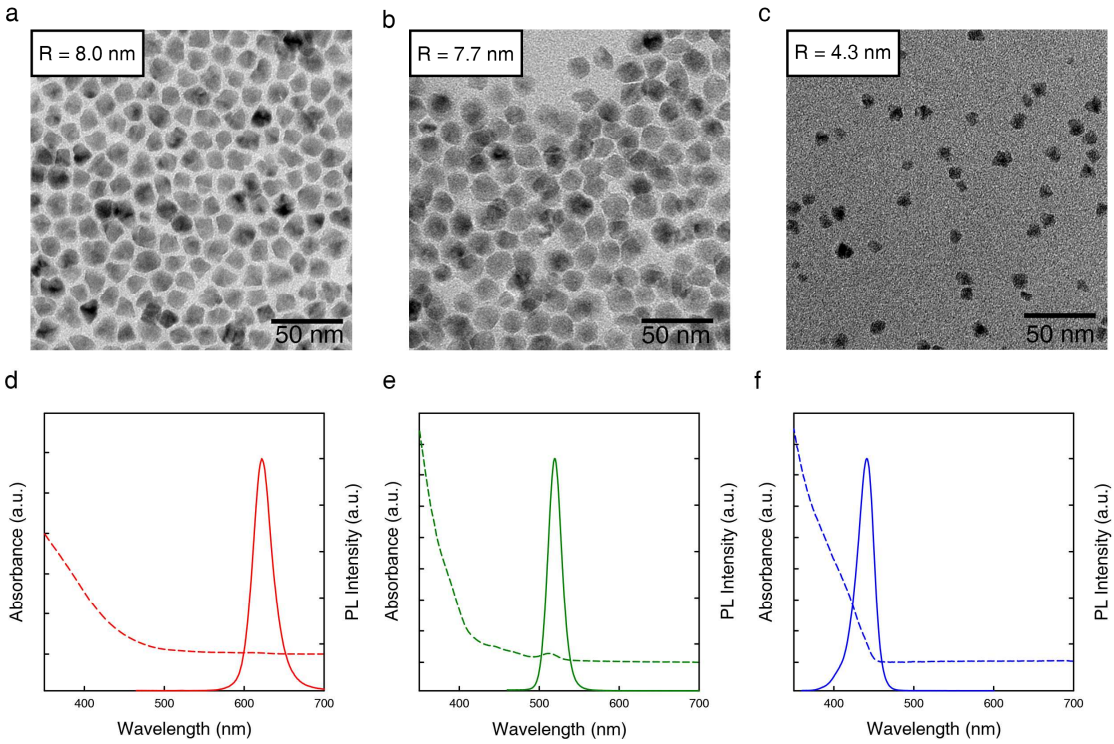

Figure S2. (a-c) High-resolution TEM images and (d-f) absorbance and photoluminescence spectra of (a, d) CdSe(r = 2 nm)/$Cd_{1-X}Zn_XS$(h = 6 nm) red-emitting QDs, (b, e) $Cd_{1-X}Zn_XSe$(r = 1.5 nm)/ZnS(h = 6.2 nm) green-emitting QDs and (c, f) $Cd_{1-X}Zn_XS$(r = 2 nm)/ZnS(h = 2.3 nm) blue-emitting QDs.

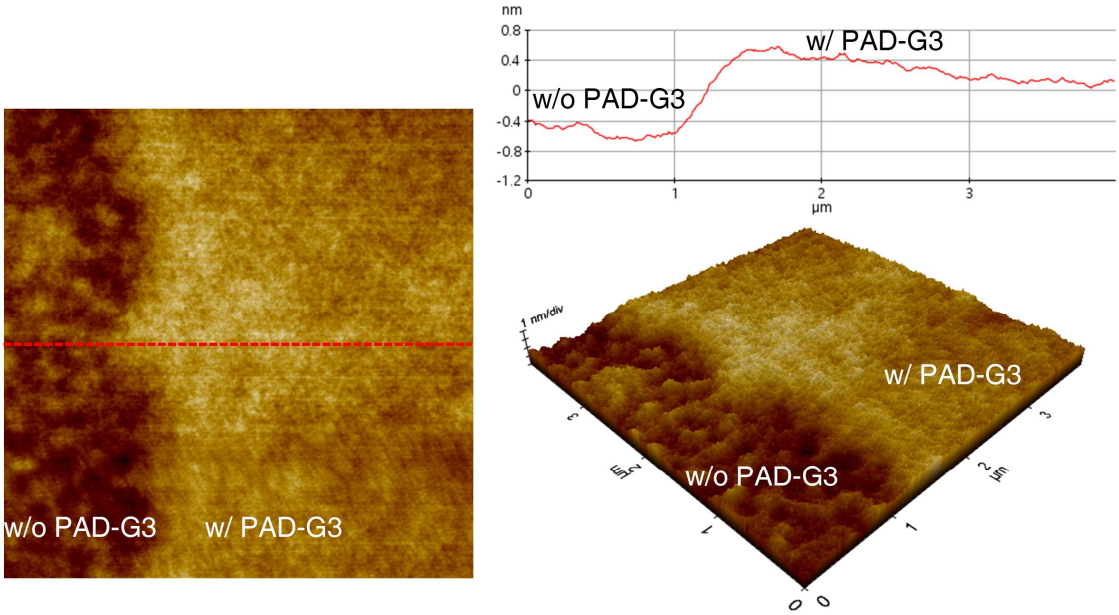

Figure S3. Atomic force microscopy (AFM) images of PAD-G3 deposited on ZnO substrate. The thickness of PAD-G3 in solid state is measured to be approximately 1 nm from the height profile across bare ZnO (w/o PAD-G3) and PAD-G3 coated ZnO (w/ PAD-G3).

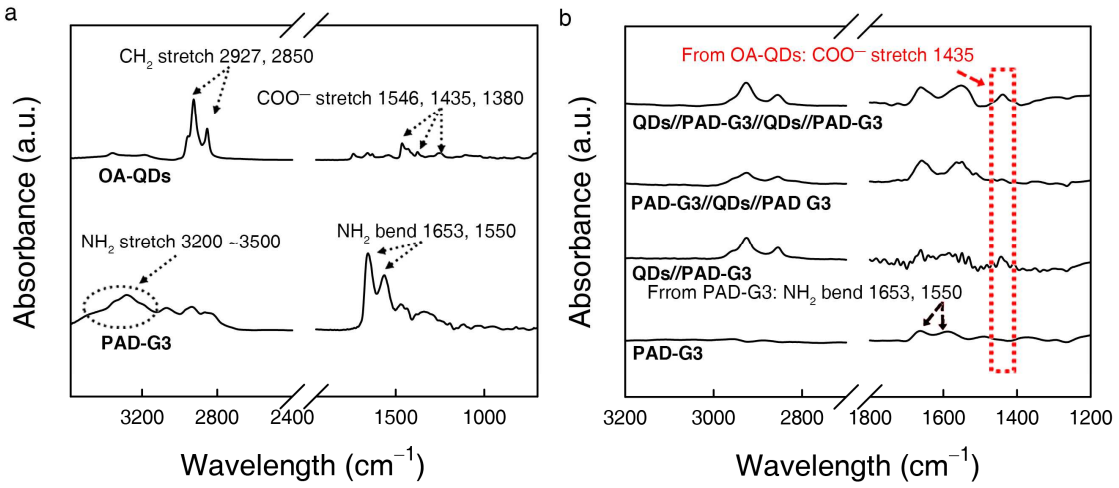

Figure S4. (a) FT-IR spectra of PAD-G3 and CdSe(r = 2 nm)/CdS(h = 6 nm) QDs. The OA-QD denotes oleic acid stabilized CdSe/CdS QDs. (b) FT-IR spectra of PAD-G3, QDs//PAD-G3, PAD-G3//QDs//PAD-G3 and QDs//PAD-G3//QDs//PAD-G3 films. FT-IR spectra of OA-QDs (*i.e.*, QDs) and PAD-G3 displayed absorption peaks corresponding to the COO^- symmetric stretching peak (1435 cm^{-1}) of OA stabilizers, and to the N–H bending vibrations of PAD-G3 (1653 and 1550 cm^{-1}), which included amine groups ($–NH_2$).[S8-S11] The alternating deposition of PAD-G3 and QDs showed inverse changes in the peak intensities of the N–H bending and COO^- symmetric stretching; that is, as the PAD-G3 layer was deposited onto the outermost QDs layer, the COO^- symmetric stretching peak of the QD stabilizers at 1435 cm^{-1} disappeared and the N–H bending peak originating from the PAD-G3 was intensified (see the FT-IR spectrum of the PAD-G3//QD//PAD-G3 in Figure S2b). For these reasons, we could confirm that PAD G3 replaced the oleic acid *via* ligand exchange due to their affinity difference and chemisorbed QDs with their amine functionality. The degree of relative conversion was calculated by comparing the FT-IR absorption peak area of OA ligand groups (at 1435cm^{-1}) as a bilayer number. In this case, a 100% conversion rate indicates that the OA ligands are completely replaced by the PAD-G3 when the outermost layer comprises the PAD-G3. The calculated degree of relative conversion was 72 %.

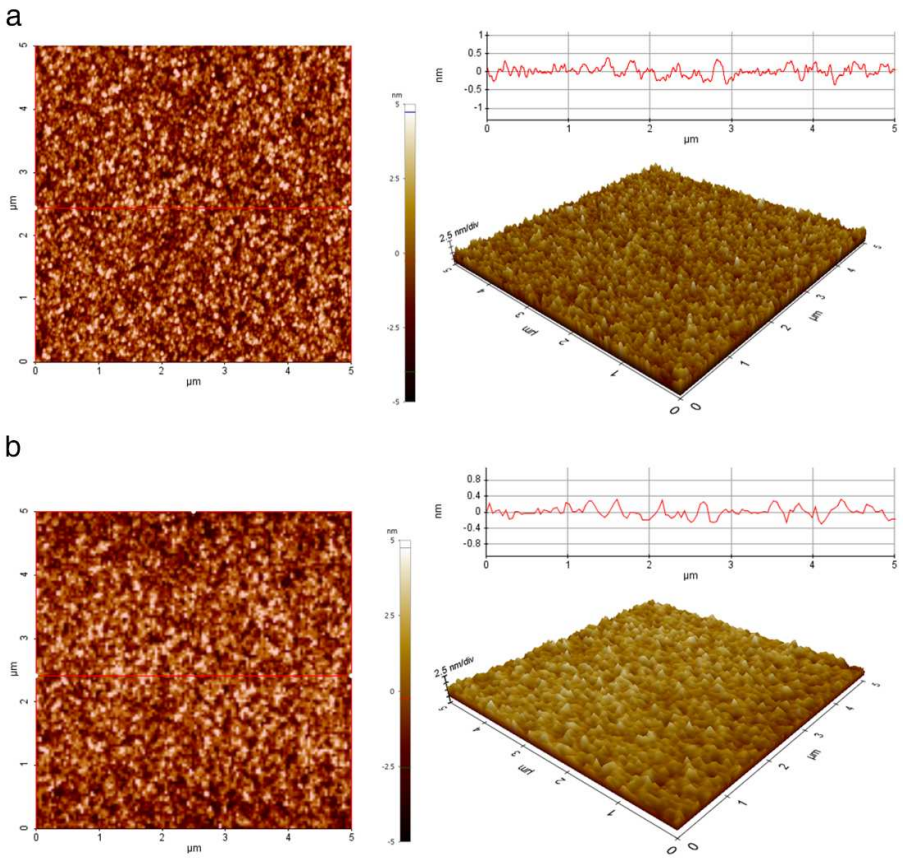

Figure S5. Atomic force microscopy (AFM) images of (a) ZnO and (b) PAD-G3//ZnO films.

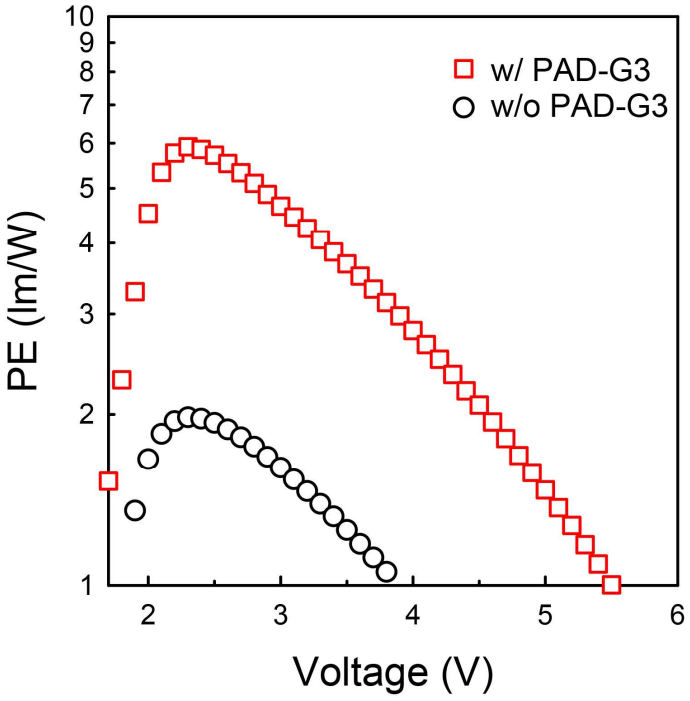

Figure S6. Power efficiency (PE) *versus* voltage of QLEDs with native ligands (w/o PAD-G3, black (empty circle)) and multi-branched dendrimer ligands (w/ PAD-G3, red (empty square)).

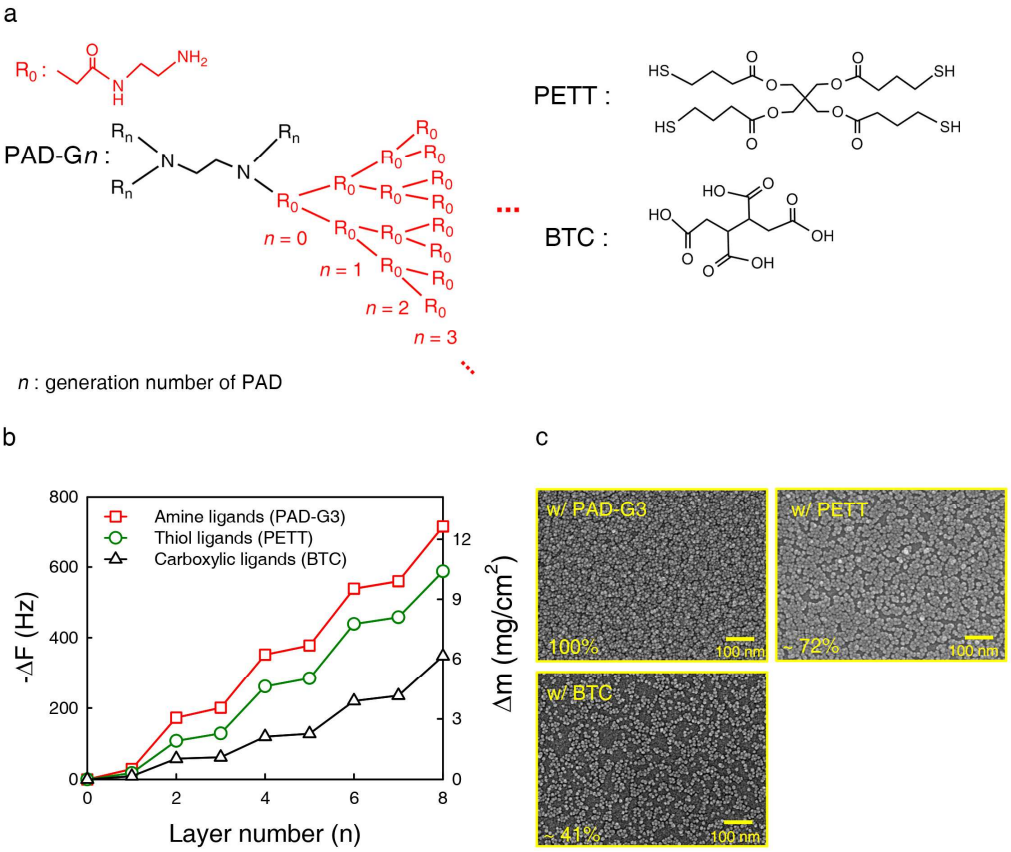

Figure S7. Chemical structures of ligands functionalized with (a) primary amine (poly(amidoamine) dendrimers (PAD), left), thiol (–SH) (pentaerythritol tetrakis (PETT), right top) and carboxylic acid (1,2,3,4-butanetetracarboxlic acid (BTC), right bottom). (b) QCM data of multilayered films comprising amine (red square), thiol (green triangle), or carboxylic acid (black circle) ligands with CdSe/CdS QDs on ZnO film (odd layer number: ligands, even layer number: QDs). (c) Top view SEM images of the QD emissive layers with PAD-G3 (top left), PETT (top right), BTC (bottom left). The QD density ratios were calculated from SEM data (w/ PAD-G3: 100%, w/ PETT: 72%, and w/ BTC: 41%).

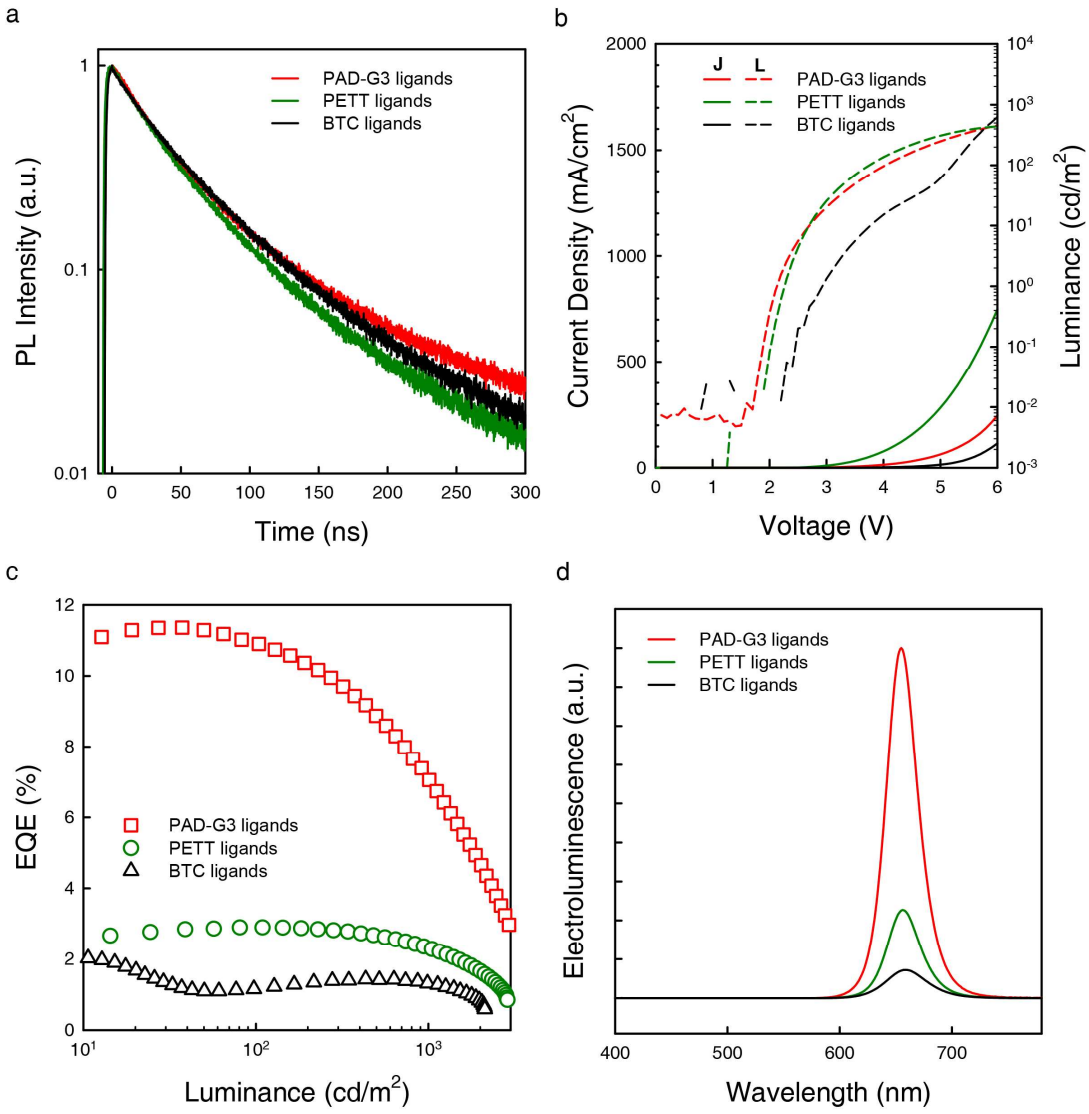

Figure S8. (a) Film PL decay dynamics of CdSe/CdS QDs on PAD-G3, PETT and BTC interfacial ligands//ZnO//ITO substrates. (b) Current density−voltage−luminance, (c) EQE *versus* luminance and (d) EL spectra (@ 10.2 mA/cm^2) of QLEDs employing CdSe/CdS QDs with PAD-G3 (red), PETT (green) and BTC ligands (black).

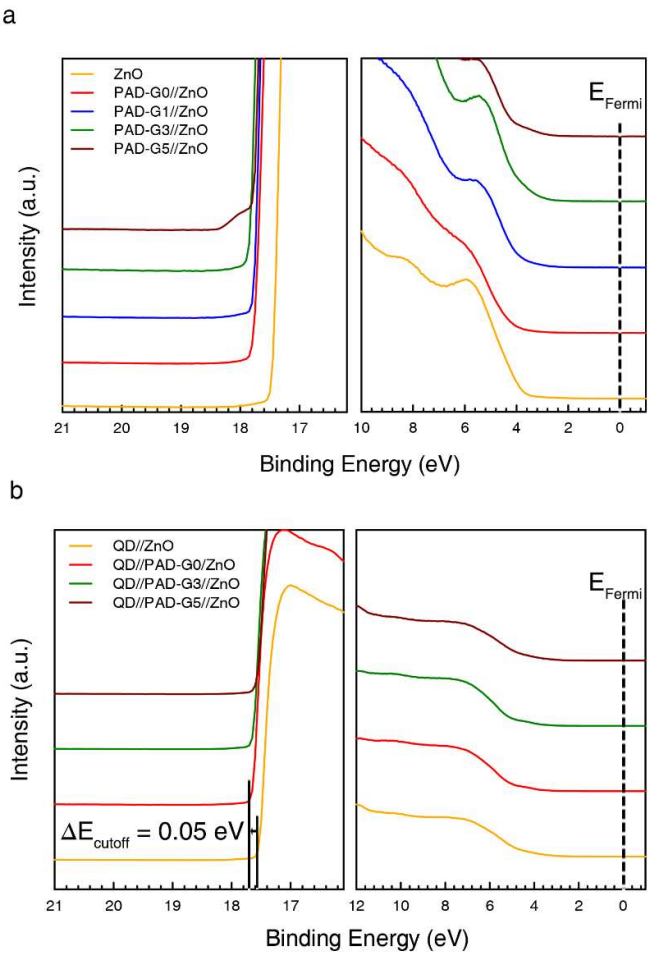

Figure S9. UPS spectra of (a) the bare ZnO film and ZnO films coated with PAD ligands and (b) QDs on the bare ZnO film and ZnO films coated with PAD ligands.

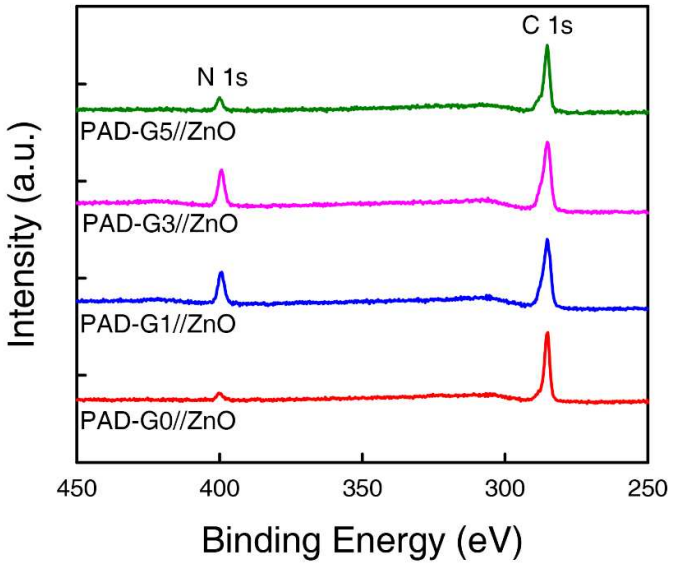

Figure S10. XPS spectra of N 1S and C 1S of ZnO films coated with PAD ligands.

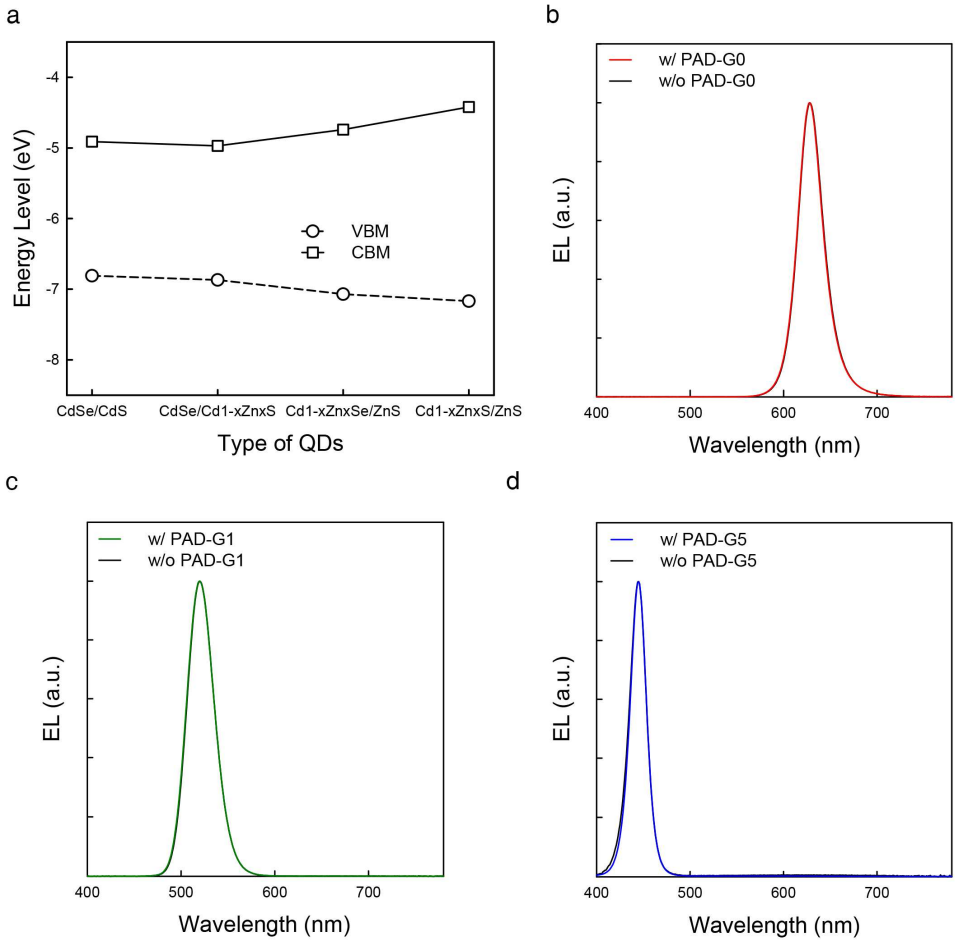

Figure S11. (a) VBM and CBM energy levels with type of QDs (CdSe(r = 2 nm)/CdS(h = 6 nm), CdSe(r = 2 nm)/$Cd_{1-X}Zn_XS$(h = 6 nm), $Cd_{1-X}Zn_XSe$(r = 1.5 nm)/ZnS(h = 6.2 nm) and $Cd_{1-X}Zn_XS$(r = 2 nm)/ZnS(h = 2.3 nm) QDs. Normalized EL spectra of QLEDs employing (b) CdSe(r = 2 nm)/$Cd_{1-X}Zn_XS$(h = 6 nm), (c) $Cd_{1-X}Zn_XSe$(r = 1.5 nm)/ZnS(h = 6.2 nm) and (d) $Cd_{1-X}Zn_XS$(r = 2 nm)/ZnS(h = 2.3 nm) QDs with PADs (w/ PAD-Gn, colored) and native ligands (w/o PADs, black).

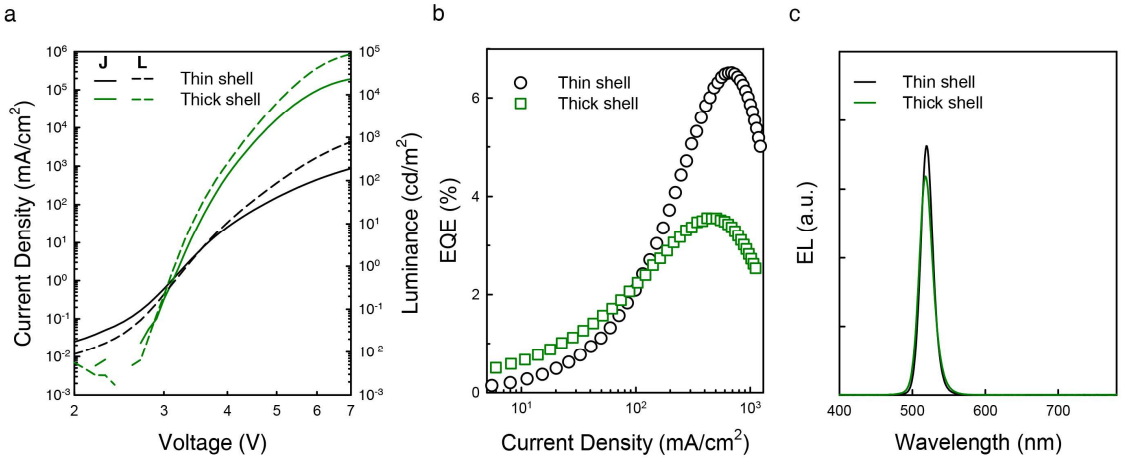

Figure S12. (a) Current density−voltage−luminance, (b) EQE *versus* current densitiy and (c) EL spectra (@ 10 mA/cm^2) of QLEDs employing $Cd_{1-X}Zn_XSe$(*r* = 1.5 nm)/ZnS(*h* = 4.2 nm) (black) and $Cd_{1-X}Zn_XSe$(*r* = 1.5 nm)/ZnS(*h* = 6.2 nm) (green) without PADs.

2. References

S1. Bae, W. K.; Padilha, L. A.; Park, Y.-S.; McDaniel, H.; Robel, I.; Pietryga, J. M.; Klimov, V. I. Controlled Alloying of the Core-Shell Interface in CdSe/CdS Quantum Dots for Suppression of Auger Recombination. *ACS Nano* **2013**, *7*, 3411–3419.

S2. Bae, W. K.; Park, Y.-S.; Lim, J.; Lee, D.; Padilha, L. A.; McDaniel, H.; Robel, I.; Lee, C.; Pietryga, J. M.; Klimov, V. I. Controlling the influence of Auger recombination on the performance of quantum-dot light-emitting diodes. *Nat. Commun*. **2013**, *4*, 2661.

S3. Lim, J.; Jeong, B. G.; Park, M.; Kim, J. K.; Pietryga, J. M.; Park, Y.-S.; Klimov, V. I.; Lee, C.; Lee, D. C.; Bae, W. K. Influence of Shell Thickness on the Performance of Light-Emitting Devices Based on CdSe/$Zn_{1-x}Cd_xS$ Core/Shell Heterostructured Quantum Dots. *Adv. Mater.* **2014**, *26*, 8034–8040.

S4. Bae, W. K.; Lim, J.; Lee, D.; Park, M.; Lee, H.; Kwak, J.; Char, K.; Lee, C.; Lee, S. R/G/B/Natrual White Light Thin Colloidal Quantum Dot-Based Light-Emitting Devices. *Adv. Mater.* **2014**, *26*, 6387–6393.

S5. Bae, W. K.; Nam, M. K.; Char, K.; Lee, S. Gram-Scale One-Pot Synthesis of Highly Luminescent Blue Emitting $Cd_{1-x}Zn_xS$/ZnS Nanocrystals. *Chem. Mater.* **2008**, *20*, 5307–5313.

S6. Kwak, J.; Bae, W. K.; Lee, D.; Park, I.; Lim, J.; Park, M.; Cho, H.; Woo, H.; Yoon, D. Y.; Char, K.; Lee, S.; Lee, C. Bright and Efficient Full-Color Colloidal Quantum Dot Light-Emitting Diodes Using an Inverted Device Structure. *Nano Lett.* **2012**, *12*, 2362–2366.

S7. Sun, Y.; Seo, J. H.; Takacs, C. J.; Seiter, J.; Heeger, A. J. Inverted Polymer Solar Cells Integrated with a Low Temperature-Annealed Sol-Gel-Derived ZnO Film as an Electron Transport Layer. *Adv. Mater.* **2011**, *23*, 1679–1683.

S8. Ko, Y.; Baek, H.; Kim, Y.; Yoon, M.; Cho, J. Hydrophobic Nanoparticle-Based Nanocomposite Films Using In Situ Ligand Exchange Layer-by-Layer Assembly and Their Nonvolatile Memory Applications. *ACS Nano* **2013**, *7*, 143–153.

S9. Kim, D.; Cheong, S.; Ahn Y. G.; Ryu, S. W.; Kim, J.-K.; Cho, J. Multicatalytic Colloids with Highly Scalable, Adjustable, and Stable Functionalities in Organic and Aqueous Media. *Nanoscale* **2015**, *8*, 7000–7016.

S10. Luther, J. M.; Law, M.; Song, Q.; Perkins, C. L.; Beard, M. C.; Nozik, A. J. Structural, Optical, and Electrical Properties of Self-Assembled Films of PbSe Nanocrystals Treated with 1,2-Ethanedithiol. *ACS Nano* **2008**, *2*, 271–280.

S11. Chen, S.; Liu, W. Oleic Acid Capped PbS Nanoparticles: Synthesis, Characterization and Tribological Properties. *Mater. Chem. Phys.* **2006**, *98*, 183–189.